Mathematical Modeling of Polyethylene Terephthalate Pyrolysis in a Spouted Bed

Arezou Niksiar, Amir Hasan Faramarzi, and Morteza Sohrabi
Chemical Engineering Dept., Amirkabir University of Technology, Tehran 15875-4413, Iran

DOI 10.1002/aic.14775
Published online March 16, 2015 in Wiley Online Library (wileyonlinelibrary.com)

A model has been developed for pyrolysis of polyethylene terephthalate (PET) in a spouted bed reactor based on the conservation equations for heat, mass, and momentum transports. A spouted bed has been constructed and the kinetic parameters have been obtained within the temperature range of 723–833 K, using two particle size ranges, (0.1–1.0) × 10^{-3} and (1.0–3.0) × 10^{-3} m. The model' predictions for the radial distributions of temperature and concentration confirm the excellent mixing of particles. Thus, spouted beds are appropriate equipments for performing kinetic studies of PET pyrolysis. The inlet gas temperature and the mass of PET highly affect PET conversion. The amount of inert particles has a negligible effect on the conversion and it can be reduced as far as a stable spouting is preserved. The gas flow suffices to eliminate the external heat and mass-transfer limitations. It can be reduced to the minimum value to decrease the energy consumption. © 2015 American Institute of Chemical Engineers *AIChE J*, 61: 1900–1911, 2015
Keywords: spouted bed, pyrolysis, PET, waste plastics, streamtube model, mathematical modeling

Introduction

Spouted bed reactors (SBRs) have been successfully applied in the study of the waste plastics pyrolysis process. The good behavior of this kind of reactors has been proven in the kinetic study of pyrolysis of biomass[1] and of waste plastics.[2] SBRs perform very well in the pyrolysis of large, sticky and irregular particles with a wide size distribution.[3] Pyrolysis occurs in the thin layers of melted plastic coating inert particles, which minimizes the diffusional restrictions and allows for reaching an isothermal regime and avoids particle agglomeration. Therefore, SBRs are appropriate alternative for performing kinetic studies of pyrolysis reactions.[4] A number of kinetic studies have been conducted in spouted bed for pyrolysis of plastic materials.[4–8] Furthermore, several experimental studies have been carried out on characterization of pyrolysis products,[9] yields of different products,[10] and the determination of suitable operating conditions[11] in SBRs. The investigations have been carried out both in batch[4,6] and continuous[12–14] operations.

In addition to experimental studies, a number of mathematical models have been presented in literature to investigate the performance of spouted beds. The computational fluid dynamic models deal with the hydrodynamic behavior of spouted beds.[15,16] Nevertheless, no comprehensive mathematical model has been yet developed to predict profiles of temperatures, concentrations, and velocities inside SBRs in the case of pyrolysis process. The available models have been developed essentially based on a number of empirical correlations for determination of the required hydrodynamic parameters. Generally, the models put forward deal with various processes including drying,[17–20] gasification,[21–23] oxidation,[24] and desulfurization.[25–27] Nevertheless, the lack of mathematical models for the pyrolysis process is evident in the literature. The authors have recently presented a comprehensive mathematical model for the pyrolysis of various waste plastic materials in SBRs.[28] In this model, the use of a bulk of empirical correlations for the evaluation of hydrodynamic parameters have been avoided, as they may impose large errors in predicting the reactor parameters.[29]

The pyrolysis of waste plastic materials in a spouted bed is a complicated process involving heat, mass and momentum transports simultaneously. In the pyrolysis of PET, a number of benzenic compounds are typically produced which are subjected to some undesired environmental impacts.[30] The toxicity of the products as well as the difficulty in providing the special operational conditions required for the pyrolysis reaction may limit the experimental investigations. In this condition, a comprehensive mathematical model could be a useful tool in getting knowledge of the process.

In the present study, the previously presented model[28] has been extended and applied to the PET pyrolysis process in a SBR. The kinetic parameters needed to solve the model have been determined experimentally in a laboratory setup consisting of a SBR. The reactor has been designed and used to study the pyrolysis process of waste plastic materials. Hence, by analyzing the results of the presented model, the performance of the SBR has been evaluated under various operating conditions.

Experimental

Materials

The PET pellets were gathered from waste beverages bottles shredded into small pieces. The pellets were slab-shaped

Correspondence concerning this article should be addressed to M. Sohrabi at sohrabi@aut.ac.ir.

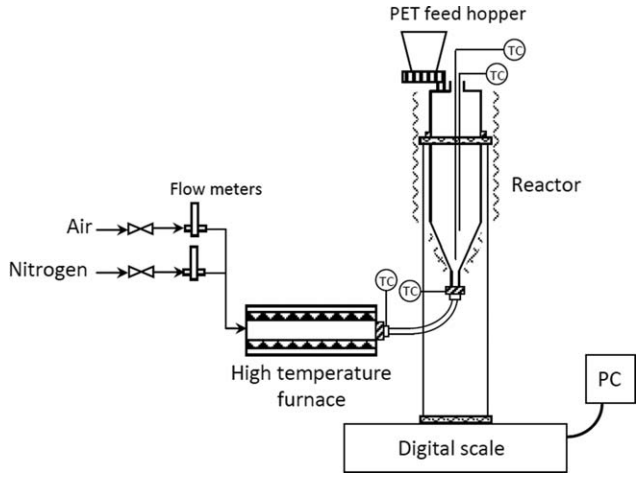

Figure 1. Schematic diagram of the pyrolysis bench scale plant.

with two size ranges, $(0.1–1.0) \times 10^{-3}$ and $(1.0–3.0) \times 10^{-3}$ m. The density of PET pellets is 1380 kg/m^3.

Experimental setup

A diagrammatic scheme of the experimental setup is shown in Figure 1. The components of the pyrolysis setup are: (1) pyrolysis reactor, (2) solid feeder, (3) system for feeding the inert gas, (4) furnace, (5) digital balance, (6) flexible duct connecting the reactor to the furnace, (7) control unit, and (8) scrubber. The SBR is of conical shape equipped with an upper cylindrical section (Figure 2). The total height of the reactor, H_t, is 0.205 m, the height of the conical section, H_c, is 0.020 m, and the angle of the conical section, γ, is 37°. The diameter of the cylindrical section, D_c, is 0.040 m, and the gas inlet diameter, D_i, is 0.010 mm.

A high-temperature tube furnace (Thermolyne 54500) was used to preheat the gas entering the reactor. The gas (nitrogen) was heated to the reaction temperature. The nitrogen flow was controlled by means of a mass flow meter (up to 0.001 m^3/s).

The reactor was placed on a digital balance, model A&D GX-2000, with the accuracy of $\pm 1 \times 10^{-5}$ kg, and the mass changes during the pyrolysis of PET were recorded continuously every 0.5 s. To increase the accuracy of data related to weight of sample, any force component between the reactor and other equipment connected to the reactor should be minimized. The major connection is the one between the preheater and the reactor. For this purpose, a flexible stainless steel tube was used (0.22 m in length, 0.008 m OD) to connect the preheater to the reactor, where its flexibility caused the forces to be balanced. The reactor and the flexible duct were carefully insulated to minimize the energy loss.

The bed temperature was measured using two thermocouples located within the reactor; the first close to the bed entrance and the second at the middle of the bed inside the mass of sand particles.

Experimental Procedure

The bed was initially consisted of 0.030 kg of sands. Sand particles $(1.19 \times 10^{-3}–1.41 \times 10^{-3}$ m) were used to ensure effective mixing of the materials inside the bed and to preserve a stable spouting regime during the pyrolysis reaction. A nitrogen flow stream with 1.2 times of the minimum spouting velocity was used to prevent defluidization phenomenon and ensure a good mixing in the bed. When the sand temperature inside the bed was stable and uniform, a mass of 0.001 kg PET was introduced to the reactor as a pulse. Since this time, the weight changes were monitored continuously. Experiments without any PET particles were carried out to examine the buoyancy effect. Preliminary tests under both cold and hot runs conditions revealed a good performance of the system during weight data collection. The pyrolysis volatile products left the reactor via a thermostated pipe and were allowed to vent to the atmosphere after passing a scrubber.

Experiments were carried out under isothermal conditions at temperatures 723, 743, 783, and 833 K. Each experimental value was repeated three times to ensure reproducibility of the bed data.

At the end of each run, a small amount of coke remained within the reactor. The coke coated uniformly around the sand particles and its mass was calculated by weighting the total amount of sand particles before and after the reaction. In general, the mass of coke produced was negligible in

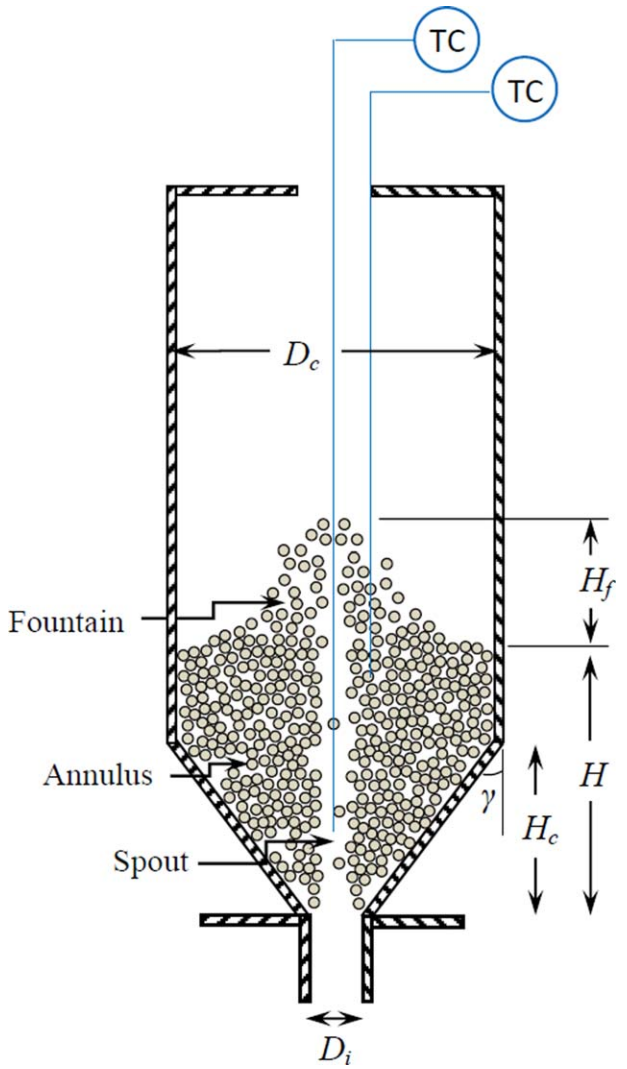

Figure 2. Schematic diagram of the SBR.

[Color figure can be viewed in the online issue, which is available at wileyonlinelibrary.com.]

comparison with the initial mass of PET used (lower than 6%).

Kinetic Model

The kinetic scheme adopted was a simple reaction model:

PET → Volatile products

The kinetic results have been correlated with the following first-order reaction scheme:

$$\frac{dX}{dt}=k(1-X) \tag{1}$$

where, X is conversion of PET defined as,

$$X=\frac{W_0-W}{W_0-W_\infty} \tag{2}$$

where, W_0, W, and W_∞ are the initial weight of sample, and the weight of that at time t during the pyrolysis and the weight at the end of the reaction, respectively.

In Eq. 1, k is expressed by the Arrhenius equation, as follows:

$$k=k_0\ \exp\left(-\frac{E}{RT}\right) \tag{3}$$

The values of activation energy and frequency factor has been obtained and presented in Table 4.

Mathematical Model

Model description

The spouted bed is modeled based on the concept of streamtube approach of Lim and Mathur.[31] The prediction accuracy of this model has been satisfactorily tested previously.[18] Three major zones have been considered in the reactor and the governing equations of heat, mass, and momentum transfers have been derived for each zone. The model's characteristics are explained as follows:

Materials

- The solid phase consisted of the inert sand particles and the unreacted waste PET
- The initial plastic materials were distributed uniformly over the sand particles throughout the bed

Heat transfer

- A heterogeneous approach (different gas and solid temperature fields) is adopted. The energy is exchanged between both phases by gas-particle heat transfer. The heat of pyrolysis reaction is assigned to the particles.
- The reactor is thermally insulated from the surrounding.

Hydrodynamic

- The diameter of the spout is unchanged and equal to the inlet diameter of bed**.**
- The fountain core is an extension of the spout zone, having the same radius.
- The foundation premium is considered as a mixed-flow media without any pyrolysis reaction.
- In the annulus, each streamtube is divided into two sections: a part of which exchanges heat, mass and momentum with the spout zone and the second has no contribution to such exchanges (Figure 4). The governing equations of mass, heat, and momentum transports are developed in two forms accordingly.

Chemical reaction

- The rate of PET pyrolysis reaction has been determined, using Eq. 1.
- The fluid-particle mass transfer and the diffusional resistances are neglected.

Model Formulization

Figure 2 shows three main regions considered in the spouted bed, i.e., the spout, the annulus, and the fountain regions. The system is composed of a gas–solid mixture, with variable compositions and temperature of both phases. To develop the mathematical model, the mass fraction of PET in the solid phase was defined as PET free basis, according to the following relation,

$$x=\frac{\dot{w}_p}{\dot{w}_{\text{sand}}} \tag{4}$$

where $\dot{w}_p$ is mass flow rate of unreacted waste plastic and $\dot{w}_{sand}$ is that of the inert sand particles.

The mass fraction of PET materials, x, could be related to the conversion of the latter, X, by the following relation:

$$1-X=\frac{W_{\text{sand}}}{W_0}x \tag{5}$$

where W_0 and W_{sand} are the mass of PET material and inert sand particles, respectively (the mass of coke was neglected).

In the gas phase, the mass fraction of volatile products is defined as:

$$y=\frac{\dot{m}_{g,i}}{\dot{m}_{g,t}} \tag{6}$$

where $\dot{m}_{g,i}$ and $\dot{m}_{g,t}$are mass flow rate of volatile gas product and the total mass flow rate of gas including that of the inert spouting gas (nitrogen), respectively.

Spout zone

In the spout zone, the gas and particles flow co–currently from bottom to the top, while the particles enter the spout from the annulus zone. Pyrolysis gas along with the carrier gas flow upward, pass the spout and enters the annulus region. Figure 3 shows a control volume of the spout region selected to develop the model.

The conservation equations developed for the gas and particle phases in the spout zone are summarized in Table 1. In these equations, R_A is the rate of pyrolysis reaction which could be substituted by the empirical rate expression deduced in the present study (*see* the Results and Discussions section).

Furthermore, the solid phase density, ρ_{p}, is expressed as the density of inert sand particles coated with molten PET, being a combination of the sand and PET densities according to the following expression:

$$\rho_{\text{p}}=\frac{\rho_{\text{sand}}\rho_t}{\rho_t+x\rho_{\text{sand}}}(1+x) \tag{7}$$

Annulus zone

The annulus zone is modeled based on the concept of streamtube approach of Lim and Mathur.[31] In this model, the

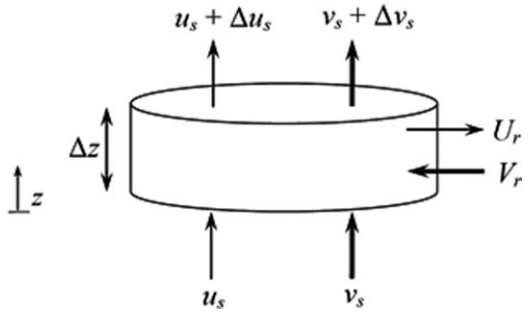

Figure 3. Selected element for spout region.

annulus is considered to consist of a series of plug–flow stream tubes (Figure 4). Each streamline exchanges energy and momentum with the other streamlines at its neighborhood. The locus of streamlines is predicted as a model's parameter by solving the rest of model's equations.[28] Although the numerical calculations become rather complicated, however, no auxiliary empirical equation is needed to predict the locus of streamlines. This may be regarded as an advantage of the present model. The conservation equations developed for the gas and particle phases in the annulus zone are summarized in Table 2.

In the presented equations for the annulus zone, E_q and F_q represent the conductive heat transfer of phase q (g for gas, and p for solid) between streamline k and the neighboring stream tubes located at the two sides around the former. The terms E_q and F_q could be determined from the following relations:

$$E_q = \frac{2\pi r_k}{r_{k-1} - r_k} \Lambda_{q,k} \left(T_{qa,k-1} - T_{qa,k} \right) \tag{8}$$

$$F_q = \frac{2\pi r_k}{r_k - r_{k+1}} \Lambda_{q,k+1} \left(T_{qa,k+1} - T_{qa,k} \right) \tag{9}$$

where, subscript k represents an arbitrary streamtube located between adjacent streamtube $k+1$ on its left and streamtube $k-1$ on its right side.

In the present model, the momentum transfer occurs by friction between adjacent streamlines. In the equations presented in Table 2, R_q and L_q refer to the momentum stress terms between the adjacent streamlines on the right and left of streamtube k, respectively ($q = p, g$):

$$R_q = 2\pi (\tau_{q,r} r)|_{r_k} \tag{10}$$

$$L_q = -2\pi (\tau_{q,r} r)|_{r_{k+1}} \tag{11}$$

where $\tau_{q,z}$ and $\tau_{q,r}$ are the normal stress and shear stress in phase q, respectively, expressed as follows:

$$\tau_{q,r} = -\left(\frac{4}{3} \mu_q + \lambda_q \right) \frac{dv_q}{dz} \tag{12}$$

$$\tau_{q,r} = -\mu_q \frac{dv_q}{dr} \tag{13}$$

Here, μ_q and λ_q are the shear and bulk viscosity of phase q, respectively, while for the gas phase $\lambda_q = 0$. These parameters are calculated from the kinetic-frictional stress model for the solid phase.

As the proposed model is one-dimensional in z direction, Eq. 13 is simply reduced to the following relation:[28]

$$\tau_{q,r} = -\mu_q \left(\frac{v_{q,ak} - v_{q,ak+1}}{r_k - r_{k+1}} \right) \tag{14}$$

Fountain core

The fountain is assumed to consist of two parts: fountain core and fountain periphery. In the fountain core, air and particles move upward cocurrently. The particles, on leaving this zone, drop down to the annulus region. It is assumed that air simply flows out of the bed. Table 3 summarizes the conservation equations developed for the gas and particle phases in the fountain core.

Fountain periphery

The fountain periphery is considered to be an ideal mixed-flow region. The mass, heat, and momentum conservation laws are applied around the entire volume of this zone. Therefore, the following equations are derived by which, the mean value of solid mass fraction ($\bar{x}_a$), mean value of solid temperature ($\bar{T}_{pa}$), and mean value of solid velocity ($\bar{v}_a$) could be determined, respectively:

$$\bar{x}_a = \frac{\sum_{z=H}^{z=H_f} r_f \rho_{pf} V'_r x_f / (1+x_f)}{\sum_{z=H}^{z=H_f} r_f \rho_{pf} V'_r / (1+x_f)} \tag{15}$$

$$\bar{T}_{pa} = \frac{\sum_{z=H_b}^{z=H_f} r_f \rho_{pf} V'_r c_p (T_{pf} - T_0)}{\sum_{z=H}^{z=H_f} r_f \rho_{pf} V'_r} + T_0 \tag{16}$$

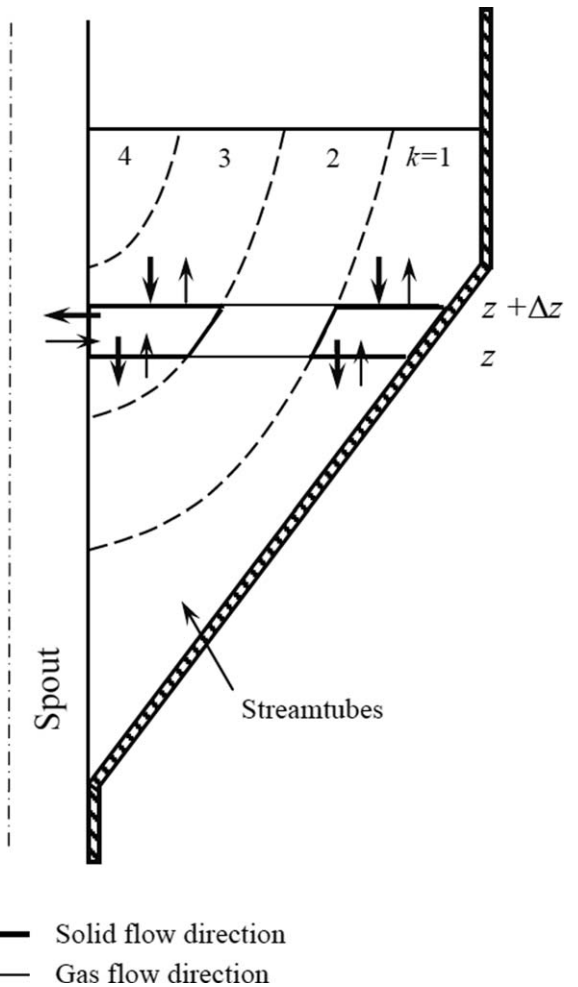

Figure 4. A control volume selected showing the solid and gas flow directions in the annulus.

Table 1. Conservation Equations for the Spout Zone in the SBR

Items considered	*Equation*
Mass transfer equations	
Gas	$\frac{dy_{s,i}}{dt}=-u_s\frac{dy_{s,i}}{dz}+\frac{R_A W_0(1-\varepsilon_{s0})}{\rho_{gs}V_{\text{sand}}\varepsilon_s}(1-y_A)$
Particles	$\frac{dx_s}{dt}=-v_s\frac{dx_s}{dz}+\frac{2V_r\rho_{pa,k}}{r_s\rho_{ps}(1-\varepsilon_s)}\left(\frac{1+x_s}{1+x_{a,k}}\right)(x_{a,k}-x_s)-\frac{R_A W_0(1-\varepsilon_{s0})}{\rho_{ps}V_{\text{sand}}(1-\varepsilon_s)}(1+x_s)$
Heat transfer equations	
Gas	$\frac{dT_{gs}}{dt}=-u_s\frac{dT_{gs}}{dz}-\frac{6h(1-\varepsilon_s)}{\varepsilon_s d_p\rho_g c_g}(T_{gs}-T_{ps})-\frac{R_A W_0(1-\varepsilon_{s0})}{\rho_g V_{\text{sand}}\varepsilon_s}(T_{gs}-T_0)$
Particles	$\frac{dT_{ps}}{dt}=-v_s\frac{dT_{ps}}{dz}+\frac{2V_r}{r_s(1-\varepsilon_s)}(T_{pa,k}-T_{ps})+\frac{6h}{d_p\rho_{ps}c_p}(T_{gs}-T_{ps})+\frac{R_A W_0(1-\varepsilon_{s0})}{\rho_{ps}c_p V_{sand}(1-\varepsilon_s)}[-\Delta H_r+c_p(T_{ps}-T_0)]$
Momentum transfer equations	
Gas	$\frac{du_s}{dt}=-u_s\frac{du_s}{dz}-\frac{\beta_s}{\varepsilon_s\rho_{gs}}(u_s-v_s)-\frac{1}{\rho_{gs}}\frac{dp}{dz}-\frac{R_A W_0(1-\varepsilon_{s0})}{\rho_{gs}V_{\text{sand}}\varepsilon_s}u_s$
Particles	$\frac{dv_s}{dt}=-v_s\frac{dv_s}{dz}-g\left(1-\frac{\rho_{gs}}{\rho_{ps}}\right)+\frac{\beta_s}{(1-\varepsilon_s)\rho_{ps}}(u_s-v_s)-\frac{1}{\rho_{ps}}\frac{dp}{dz}+\frac{R_A W_0(1-\varepsilon_{s0})}{\rho_{ps}V_{\text{sand}}(1-\varepsilon_s)}v_s$

$$\bar{v}_a=\frac{\sum_{z=H}^{z=H_f}2\pi r_f\rho_{pf}V'_r\Delta z}{A_b\rho_a(1-\varepsilon_a)} \tag{17}$$

Auxiliary Equations

Hydrodynamic parameters

The annulus voidage is taken to be constant and equal to the minimum fluidization void fraction ($\varepsilon_a=\varepsilon_{mf}$).[32] In the literature, the minimum fluidization void fraction has been given within the range of 0.42–0.45.[21,24,26]

Furthermore, the fluid–particle interaction has been taken from the model of Gidaspow,[33] being a combination of Wen and Yu model ($\beta_{\text{Wen-Yu}}$)[34] in corporating Ergun relation (β_{Ergun}):[35]

$$\beta_{\text{Ergum}}=150\frac{(1-\varepsilon)^2\mu_g}{\varepsilon(d_p)^2}+1.75\frac{\rho_g(1-\varepsilon)|u-v|}{d_p} \tag{18}$$

$$\beta_{\text{Wen-Yu}}=\frac{3}{4}C_D\frac{\rho_g(1-\varepsilon)|u-v|}{d_p}\varepsilon^{-2.65} \tag{19}$$

Thus, the exchange coefficient (β) is expressed as:

$$\beta=(1-\varphi)\beta_{\text{Eegun}}+\varphi\beta_{\text{Wen-Yu}} \tag{20}$$

Table 2. Conservation Equations for the Annulus Zone in the SBR

Items considered	Equation
Mass transfer equations	
Gas	$\frac{dy_{ak,i}}{dt}=-u_{ak}\frac{dy_{ak,i}}{dz}+\frac{2\pi r_s U_r}{A_{ak}\varepsilon_a}\alpha(y_s-y_{ak,i})+\frac{R_A W_0(1-\varepsilon_a)}{\rho_{ga,k}V_{\text{sand}}\varepsilon_a}(1-y_A)$
Particles	$\frac{dx_{a,k}}{dt}=v_{ak}\frac{dx_{a,k}}{dz}-\frac{R_A W_0}{\rho_{pa,k}V_{\text{sand}}}(1+x_{a,k})$
Heat transfer equations	
Gas	$\frac{dT_{ga,k}}{dt}=-u_{ak}\frac{dT_{ga,k}}{dz}+\frac{2\pi r_s U_r\alpha}{A_{ak}\varepsilon_a}(T_{gs}-T_{ga,k})-\frac{6h(1-\varepsilon_a)}{\varepsilon_a d_p\rho_{ga,k}c_g}(T_{ga,k}-T_{pa,k})-\frac{R_A W_0(1-\varepsilon_{a0})}{\rho_{ga,k}V_{sand}\varepsilon_a}(T_{ga,k}-T_0)+\frac{E_g+F_g}{\rho_{ga,k}c_g A_{ak}\varepsilon_a}$
Particles	$\frac{dT_{pa,k}}{dt}=v_{ak}\frac{dT_{pa,k}}{dz}+\frac{6h}{d_p\rho_{pa,k}c_p}(T_{ga,k}-T_{pa,k})+\frac{R_A W_0}{\rho_{pa,k}c_p V_{\text{sand}}}[-\Delta H_r+c_p(T_{pa,k}-T_0)]+\frac{E_p+F_p}{\rho_{pa,k}c_p A_{ak}(1-\varepsilon_a)}$
Momentum transfer equations	
Gas	$\frac{du_{ak}}{dt}=-u_{ak}\frac{du_{ak}}{dz}-\frac{\beta_{ak}}{\varepsilon_a\rho_{ga,k}}(u_{ak}+v_{ak})-\frac{1}{\rho_{ga,k}}\frac{dp}{dz}-\frac{R_A W_0(1-\varepsilon_a)}{\rho_{ga,k}V_{\text{sand}}\varepsilon_a}u_{ak}+\frac{R_g+L_g}{\rho_{ga,k}A_{ak}\varepsilon_a}$
Particles	$\frac{dv_{a,k}}{dt}=-v_{a,k}\frac{dx_{a,k}}{dz}-g(1-\rho_{ga,k}/\rho_{pa,k})+\frac{\beta_{ak}}{(1-\varepsilon_a)\rho_{pa,k}}(u_{a,k}+v_{a,k})-\frac{1}{\rho_{pa,k}}\frac{dp}{dz}+\frac{R_A W_0}{\rho_{ps}V_{\text{sand}}}v_{a,k}-\frac{1}{(1-\varepsilon_a)\rho_{pa,k}A_{a,k}}\frac{d(\tau_{zz}A_{a,k})}{dz}+\frac{R_p+L_p}{\rho_{pa,k}A_{ak}(1-\varepsilon_a)}$

Table 3. Conservation Equations for the Fountain Core Zone in the SBR

Items considered	Equation
Mass transfer equations	
Gas	$\frac{dy_f}{dt}=-u_f\frac{dy_f}{dz}+\frac{R_A W_0(1-\varepsilon_{f0})}{\rho_{gf}V_{\text{sand}}\varepsilon_f}(1-y_A)$
Particles	$\frac{dx_f}{dt}=-v_f\frac{dx_f}{dz}-\frac{R_A W_0(1-\varepsilon_{f0})}{\rho_{pf}V_{\text{sand}}(1-\varepsilon_f)}(1+x_f)$
Heat transfer equations	
Gas	$\frac{dT_{gf}}{dt}=-u_f\frac{dT_{gs}}{dz}-\frac{6h(1-\varepsilon_s)}{\varepsilon_f d_p\rho_{gf}c_g}(T_{gf}-T_{af})+\frac{R_A W_0(1-\varepsilon_f)}{\rho_{gf}\varepsilon_f V_{\text{sand}}}(T_{pf}-T_0)$
Particles	$\frac{dT_{pf}}{dt}=-v_f\frac{dT_{pf}}{dz}+\frac{6h}{d_p\rho_{pf}c_p}(T_{gf}-T_{pf})+\frac{R_A W_0}{\rho_{gf}\varepsilon_f V_{\text{sand}}}[-\Delta H_r+c_p(T_{pf}-T_0)]$
Momentum transfer equations	
Gas	$\frac{du_f}{dt}=-u_f\frac{du_f}{dz}-\frac{\beta_f}{\varepsilon_f\rho_{gf}}(u_f-v_f)-\frac{R_A W_0(1-\varepsilon_{f0})}{\rho_{gf}V_{\text{sand}}\varepsilon_f}u_f$
Particles	$\frac{dv_f}{dt}=-v_f\frac{dv_f}{dz}-g(1-\frac{\rho_{gf}}{\rho_{pf}})+\frac{\beta_f}{(1-\varepsilon_f)\rho_{pf}}(u_f-v_f)+\frac{R_A W_0(1-\varepsilon_{f0})}{\rho_{pf}V_{\text{sand}}(1-\varepsilon_f)}v_f$

The drag coefficient (C_D) is determined by the following equation:[36]

$$C_D=\begin{cases}\dfrac{24}{\text{Re}_p}[1+0.15(\text{Re}_p)^{0.687}] & (\text{Re}_p<1000)\\ 0.44 & (\text{Re}_p>1000)\end{cases} \quad (21)$$

where φ in Eq. 20 is defined as follows,

$$\varphi=\frac{\arctan[150\times1.75(0.2-(1-\varepsilon))]}{\pi}+0.5 \quad (22)$$

Heat-transfer parameters

- The heat of endothermic pyrolysis reaction of PET is $\Delta H_r = 214350$ J/kg[37]
- Gas–particle heat exchange in the spout and fountain[38]

$$\frac{hd_p}{\lambda_g}=\frac{2}{1-(1-\varepsilon)^{1/3}}+\frac{0.61}{\varepsilon}\text{Pr}^{1/3}\text{Re}^{0.55} \quad (23)$$

- Gas–particle heat exchange in the annulus:[39]

$$h=0.255\frac{\lambda_g}{\varepsilon_a d_p}\text{Pr}^{1/3}\text{Re}^{2/3} \quad (24)$$

- Conductive heat transfer coefficient between two adjacent streamlines:[40]

$$\Lambda=\frac{\lambda_q^*(1-\varepsilon)^{1/3}}{0.73869d_p} \quad (25)$$

where λ_q^* is the effective thermal conductivity that may be calculated from. [41]

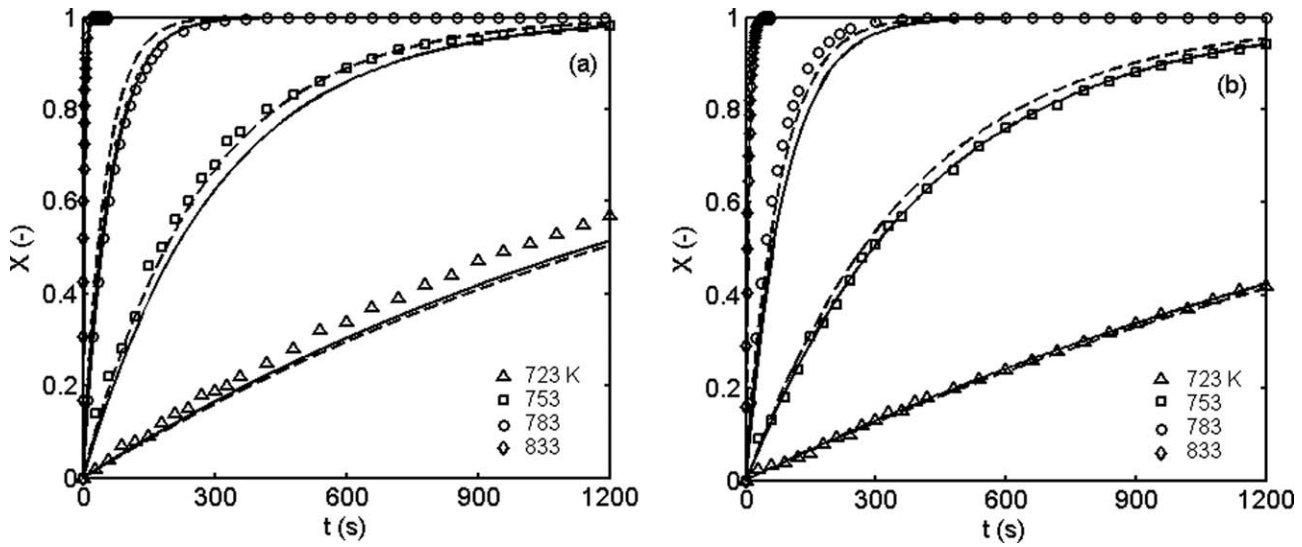

Figure 5. Evaluation of conversion of PET with time in the spouted bed for two particle size: (a) (0.1–1.0) × 10^{-3} m, (b) (1.0–3.0) × 10^{-3} m.

Solid lines: spouted bed model results for the average values, Broken lines: best fit for the kinetic data with a first-order reaction model, Points: experimental data.

Table 4. Kinetic Parameters Obtained for Pyrolysis of PET

Particle size (m)	E (J/mol)	k_0 (s^{-1})
$(0.1–1.0) \times 10^{-3}$	276,800	5.90×10^{16}
$(1.0–3.0) \times 10^{-3}$	264,300	5.53×10^{15}

Boundary Conditions

- At the bottom of the bed, the gas is being injected into the reactor in the axial direction with velocity of U_{in} and temperature T_{gin}.
- The pressure is set at atmospheric pressure on the top of the freeboard.
- The particles entering the streamtube at the top of the annulus region have a uniform mass fraction of $\bar{x}_a$, uniform temperature of $\bar{T}_{pa}$, and uniform velocity of $\bar{v}_a$, calculated from Eqs. 15, 16, and 17, respectively.
- Along the first streamtube located adjacent to the spouted bed wall, the particles' velocity at the wall (v_{a0}) and the gas velocity at the wall (u_{a0}) are both assumed to be zero (no slip boundary conditions). For this streamtube, $E_q = 0$ in Eq. 8, as the reactor walls are thermally insulated from the surrounding.

Table 5. Operating Conditions Used (Base Values)

Parameter	*Value*
Static bed height (m)	0.037
Diameter of sand particles (m)	$(1.19–1.41) \times 10^{-3}$
Size of plastic particles (m)	$(0.1–1.0) \times 10^{-3}$, $(1.0–3.0) \times 10^{-3}$
Bed temperature (K)	723–833
Inlet gas temperature (K)	723–833
Gas flow rate	1.2 times of the minimum spouting value
Mass of sand particles (kg)	0.030
Mass of PET material (kg)	0.001
Density of PET material (kg/m^3)	1380
Specific heat of PET (J/kg°C)	1440

Results and Discussions

Kinetics of PET pyrolysis

The kinetic results determined in the temperature range of 723–833 K and for two particle size ranges, that is, $(0.1–1.0) \times 10^{-3}$ and $(1.0–3.0) \times 10^{-3}$ m, have been correlated with a first-order reaction rate model. The results for the best fit are shown by the broken lines in Figure 5. In addition, the

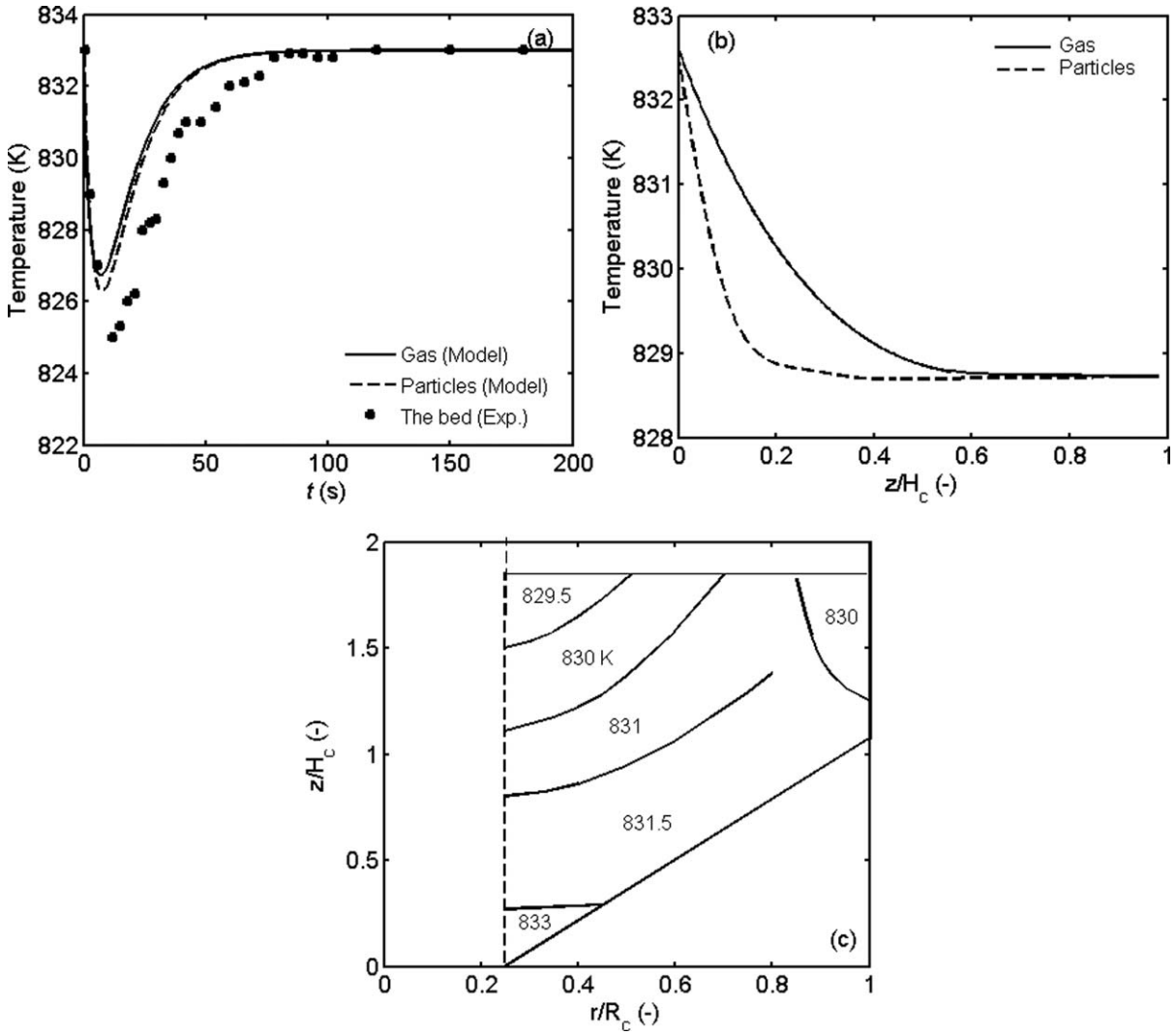

Figure 6. Profiles in the bed at $T_{gin} = 833$ K and $0.001 < d_p < 0.003$ m.

(a) Temperature change of the bed with time at $z = 0.01$ m in the spout (b) variation of gas and particle temperature along the spout length at $t = 30$ s, (c) profiles of gas temperature in the annulus at $t = 30$ s.

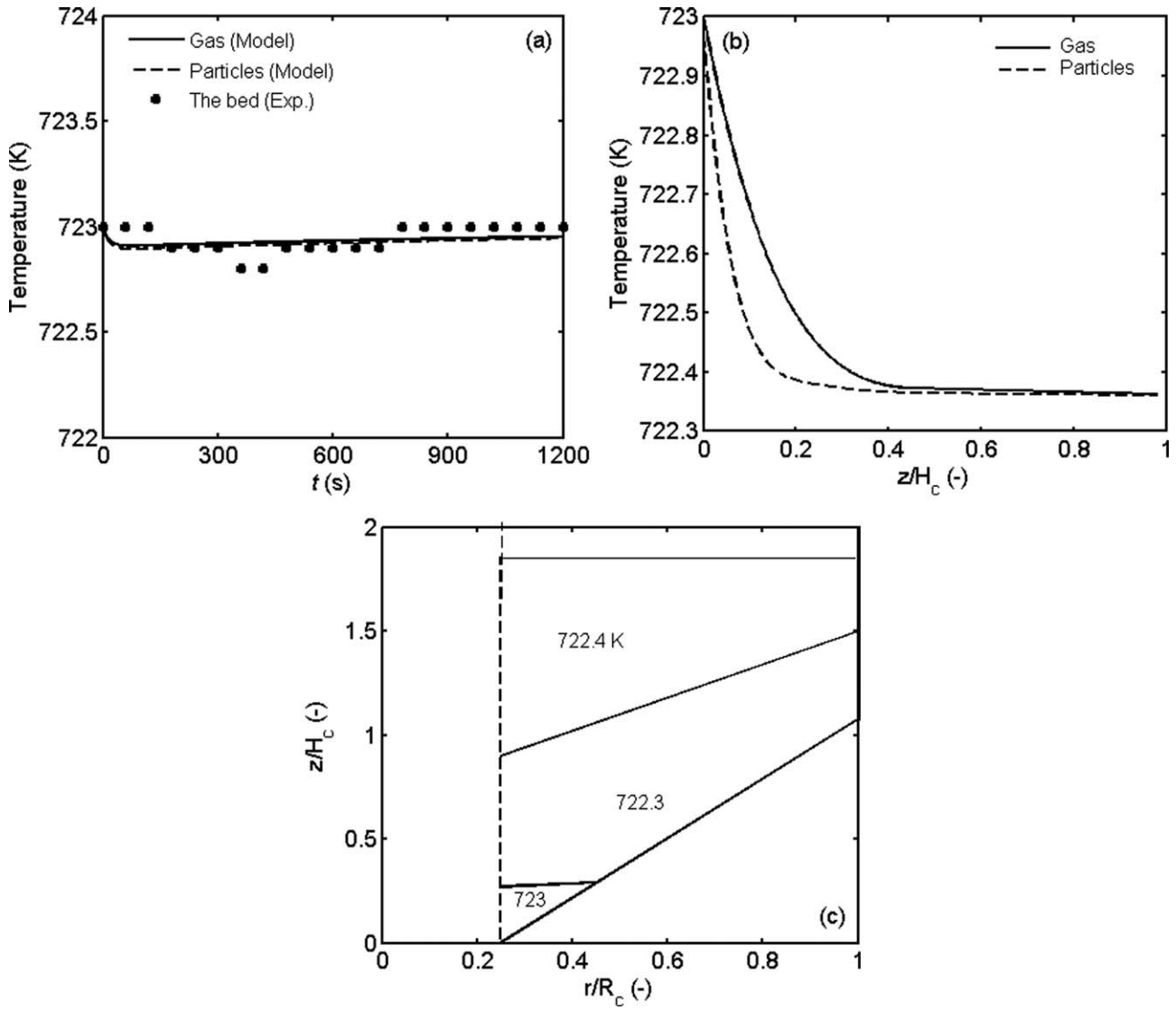

Figure 7. Profiles in the bed at $T_{gin} = 723$ K and 0.001< d_p <0.003 m.

(a) Temperature change of the bed with time at $z = 0.01$ m in the spout, (b) variation of gas and particle temperature along the spout length at $t = 480$ s, and (c) profiles of gas temperature in the annulus at $t = 480$ s.

values for activation energy and frequency factor are presented in Table 4.

Various profiles within the reactor

In this section, profiles of the reactor have been obtained and evaluated at various operating conditions. A set of operating conditions have been considered as the base values, according to Table 5. These values correspond to those applied in the laboratory experiments.

Figure 5 shows the values predicted by the model for the average conversion of PET within the bed at different temperatures (the solid lines). The experimental data for the PET conversion are shown in Figure 5 by the symbols. Two panels of this figure correspond to the two particle size ranges studied, namely $(0.1–1.0) \times 10^{-3}$ and $(1.0–3.0) \times 10^{-3}$ m Furthermore, in Figure 5, the results of the best fit for the experimental data with the kinetic parameters are shown by the broken lines. As it is observed, the model presented for the spouted bed performance provides reasonably good predictions for the PET conversion. A comparison between the results of Figures 5a, b indicates that, in the present conditions, the particle size has no remarkable effect on the conversion of PET. Generally, the heat transfer coefficient of particles, h, in SBRs is large due to the excellent mixing of the particles and the high gas flow rate.[42] In such a situation, the heat and mass-transfer limitations may be neglected and the pyrolysis reaction rate may be limited by the chemical reaction. Therefore, as it is seen in Figure 5, the particle size does not affect the reaction rate significantly.

The particle size greater than 0.001 m makes the process more feasible due to the lower energy requirements for cryogenic milling. Thus, for industrial applications of a continuous process, the results corresponding to the larger particle sizes (between 0.001 and 0.003 m) are more suitable. Figure 6 shows the various profiles in the reactor predicted by the model where the inlet gas temperature was $T_{gin} = 833$ K and the particle sizes are in the range of 0.001–0.003 m. Figure 6a illustrates the change in the gas and particle temperatures over time at a certain position in the spout ($z = 0.01$ m).

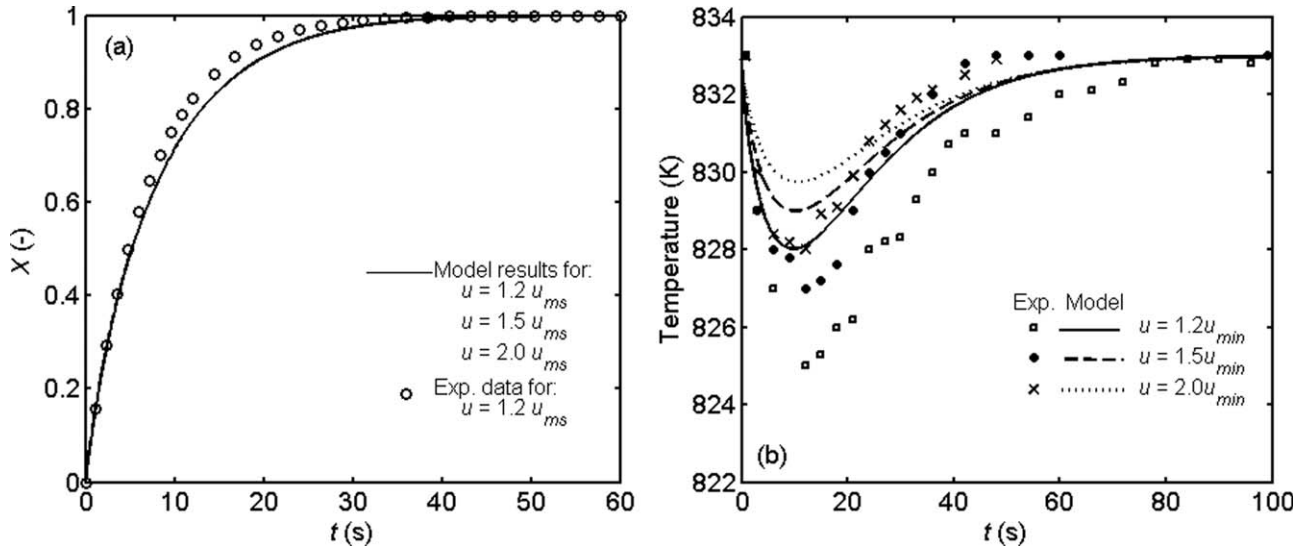

Figure 8. Effect of gas flow rate on variations of (a) mean PET conversion with time, and (b) bed temperature change with time at $z = 0.01$ m.

Lines: Model results, Points: Experimental data ($T_{gin} = 833$ K, $0.001 < d_p < 0.003$ m, $W_0 = 0.001$ kg).

This is where the bed temperature has been measured experimentally, so, a comparison could be made between the model's results and the experimental data. A rapid temperature drop has been observed at the beginning of the process due to the endothermic nature of pyrolysis reaction. The temperature drop is recovered over time by the hot flowing gas entering the reactor making the bed to tend to the isothermal conditions. The model predicts the temperature change reasonably well. Figure 6b shows the gas and solid temperature profiles along the spout length at time $t = 30$ s from beginning of the process. The particles temperature decreases slightly along the spout because heat is absorbed from the gas. The gas and particle temperatures become almost equal at the top of the bed.

Figure 6c shows the profile of gas temperature at various positions in the annular zone at $t = 30$ s. The profile for the solid temperature was equal to that of the gas (not plotted). The gas temperature drops from the inlet value (833 K) along a short distance from the entrance. Then, the temperature is increased slightly due to contacting with the hot circulating particles at the upper sections of the bed.

Figure 7 shows various profiles of the reactor predicted by the model where $T_{gin} = 723$ K: (a) the change in the gas and particle temperatures over time at a certain position in the spout ($z = 0.01$ m), (b) the gas and solid temperature profiles along the spout length at time $t = 480$ s, and (c) the profile of gas temperature at various positions in the annular zone at $t = 480$ s. In Figure 7a, the model predictions for the trend of temperature change of gas and particles inside the bed are

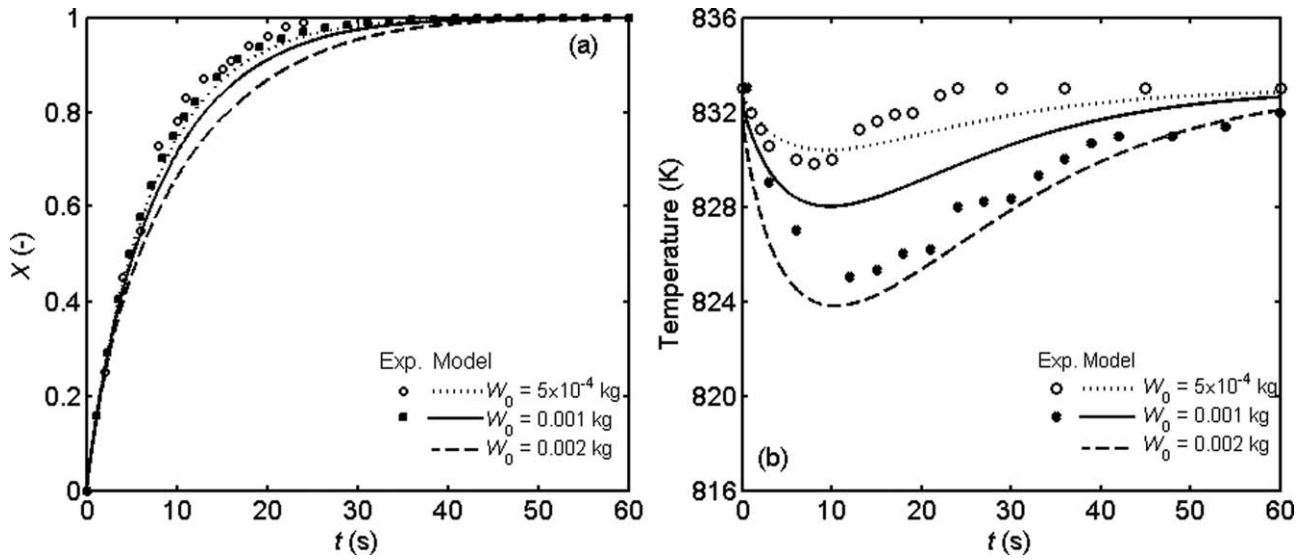

Figure 9. Effect of initial mass of PET on variations of (a) PET conversion, and (b) bed temperature change with time at $z = 0.01$ m.

Lines: Model results, Points: Experimental data ($T_{gin} = 833$ K, $0.001 < d_p < 0.003$ m, $u = 1.2\ u_{ms}$).

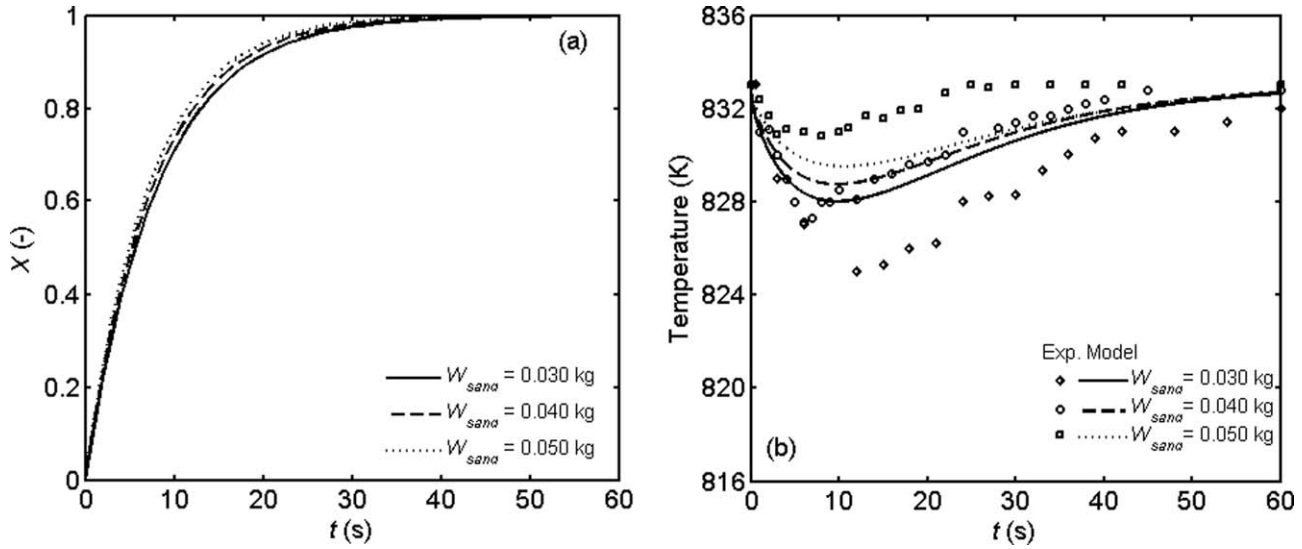

Figure 10. Effect of initial mass of sand particles on variations of (a) PET conversion and (b) bed temperature change with time at $z = 0.01$ m.

Lines: Model results, Points: Experimental data ($T_{gin} = 833$ K, $0.001 < d_p < 0.003$ m, $u = 1.2\ u_{ms}$, $W_0 = 0.001$ kg).

similar to that observed in the case of inlet gas temperature of 833 K. However, the temperature drop is less than that of the previous case (*see* Figure 6). This is because the reaction rate is smaller at a lower bed temperature. The model predictions have been compared with the measured values. As could be seen, a satisfactory agreement has been observed with an average error of 0.08%. The maximum error is 0.16%. According to Figure 7c, the temperature gradient in the annulus region is negligible.

The Effects of Operating Conditions on Pyrolysis Conversion

Effect of gas flow rate

The effect of gas flow has been studied and shown in Figure 8. Figure 8a shows that by increasing the gas flow rate from the base value of 1.2 times of the minimum spouting value, the conversion of PET does not change appreciably. In the present model, the effect of external heat and mass-transfer resistances on the conversion of the pyrolysable materials has not been considered as the process is controlled by the chemical reaction. Therefore, the gas flow rate may only affect the temperature of the bed. This is demonstrated in Figure 8b. Referring to this figure, it may be observed that the rapid temperature drop due to endothermic nature of pyrolysis reaction is almost similar in all three case studied. When the gas flow rate is high, the temperature drop is recovered more rapidly by the hot flowing gas. However, such a fast temperature recovering does not influence the rate of reaction as the reaction has been almost completed. In Figure 8, the values predicted by model are compared with the measured values. A satisfactory agreement has been achieved with a maximum 0.5% error.

Effect of initial mass of PET

The mass of inert sand particles in the reactor in all experimental runs in this section was 0.030 kg. Here, the effect of the initial mass fraction of PET in the reactor has been investigated (Figure 9). Figure 9a shows that the conversion of PET in the spouted bed changes significantly by the change in the mass of PET initially fed to the reactor. This is due to requirement of higher energy for the pyrolysis of higher mass of PET, which causes a rapid temperature drop within the bed. This is shown in Figure 9(b). Such a fact has been considered carefully when determining the kinetic parameters in the SBR. Furthermore, measured values for bed conversion and bed temperature at $z = 0.01$ m are shown in Figures 9a and b, respectively. The data have been obtained for $W_0 = 5 \times 10^{-4}$ and 0.001 kg. For larger masses of PET ($W_0 = 0.002$ kg), some defluidization problems have been observed under the present operating conditions. Therefore, the experimental data could not be obtained for $W_0 = 0.002$ kg. As could be seen in Figure 9, a reasonably good agreement has been achieved between the model results and the experimental data. The maximum error is 0.2%.

Effect of inert sand mass

The initial mass fraction of PET material was kept unchanged at 0.001 kg while the mass of inert sand particles in the reactor was varied. In Figure 10a, the variation of PET conversion, and in Figure 10b, the variation of bed temperature with time are plotted. Different masses of sand (0.030, 0.040, and 0.050 kg) were applied. In all cases, the gas flow rate was adjusted at 1.2 times of the minimum spouting value. The gas flow rate was changed according to the increasing mass of sands particles. The results revealed that conversion of PET changes slightly with different mass of sand particles. By increasing the mass of inert particles from 0.030 to 0.050 kg, the static bed height was also increased. However, the circulation rate of the particles throughout the bed may not have been changed appreciably, as the gas flow rate was enhanced to higher values at the same time. The only difference is the required heat of pyrolysis reaction which was supplied by a larger mass of particles. As the result, the temperature change of the particles bed is lower. From Figure 10b, it is evident that in the presence of larger mass of sands particles, the temperature change of the bed is rather low. This may lead to a higher isothermicity of the bed and a better spouted-bed

performance. Nevertheless, the improvement of PET conversion is rather negligible (Figure 10a). This is also important to note that larger amounts of inert particles require higher energy to be supplied from the gas flow to preserve a stable spouting operation. Such a fact has to be considered in design of SBRs.

Conclusion

A kinetic study has been performed for pyrolysis of PET in a bench-scale SBR. The weight change of PET sample has been monitored continuously during the pyrolysis reaction as a novel technique and a first-order kinetic rate model has been established. A mathematical model based on the mass, heat, and momentum conservation equations, has been developed for pyrolysis of PET in spouted-bed reactors under unsteady-state conditions. The results predicted from the model have been compared with the experimental data obtained for PET conversion, and bed temperature in the SBR. A satisfactory good agreement has been observed.

According to the model's results obtained, spouted beds are suitable equipment for performing kinetic studies, as the excellent mixing and high circulation rates of the materials being occurred which temper the temperature gradient inside the reactor. This advantage minimizes the limitations of the external heat and mass-transfer resistances. Increasing the gas flow rate up to a minimum value required to preserve the spouting conditions, has no appreciable effect on the rate of reaction. Conversion of PET in SBR declined significantly by increasing the mass of PET initially fed to the reactor. This is due to a large and rapid temperature drop of the bed as the result of endothermic pyrolysis reaction. PET conversion is slightly improved by increasing the mass of inert sand particles in the bed. However, the amount of inert particles used can be reduced as far as a stable spouting condition is preserved.

Notation

A_{ak}, A_f, A_s = cross-sectional area of streamtube k in annulus, of fountain core, and of spout, respectively (m^2)
C_D = drag coefficient
c_g,c_p = specific heat of gas and solid, respectively (J/kg.K)
D_b, D_o, D_i = upper diameter of the stagnant bed, of the bed bottom, and of the bed inlet, respectively (m)
d_p = particle diameter (m)
d_s = diameter of spout (m)
E = activation energy (J/mol)
E, F = conductive heat transfer between adjacent streamlines given by Eqs. 8 and 9, respectively (W/m)
g = gravitational constant (m/s^2)
H, H_f = height of the stagnant bed, and of fountain, respectively (m)
h = gas-solid convective heat transfer coefficient ($W/m^2.K$)
k_{max} = total number of streamtubes considered in the model
L = fictional stress between adjacent streamlines given by Eq. 11 (N/m)
$\dot{m}_{g,i}$ = mass flow rate of individual gas product i (kg/s)
$\dot{m}_{g,t}$ = total mass flow rate of gas (kg/s)
Pr = Prandtl number (-)
p = pressure (Pa)
R = fictional stress between adjacent streamlines given by Eq. 10 (N/m)
R_A = rate of pyrolysis reaction (kg/kg.s)
Re_p = particle Reynolds number in Eq. 21, $Re_p = |u-v|\rho_g d_p \varepsilon/\mu_g(-)$
r = radial coordinate (m)
r_f,r_s, r_k = radius of fountain core, and of spout, and of streamtube k (m)
T_g, T_p = gas and solid temperature, respectively (K)
$\bar{T}_{pa}$ = average solid temperature at the top of bed (K)
T_0 = reference temperature (K)
t = time (s)
U_r = radial gas velocity at the spout-annulus interface (m/s)
U'_r = radial gas velocity at the interphase between fountain core and fountain periphery (m/s)
u = interstitial gas velocity (m/s)
V_r = radial particle velocity at the spout-annulus interface (m/s)
V'_r = radial particle velocity at the interphase between fountain core and fountain periphery (m/s)
V_{sand} = volume of entire sand particles (m^3)
v, $\bar{v}_a$ = interstitial solid velocity, and average value at the top of bed (m/s)
W_0 = initial mass of waste plastic (kg)
W_{sand} = mass of entire sand particles (kg)
$\dot{w}_p$, $\dot{w}_{sand}$ = mass flow rate of unreacted waste plastic, and inert sand particles, respectively (kg/s)
X = conversion degree of plastic material (kg/kg)
x, $\bar{x}_a$ = mass fraction of waste plastic in plastic free basis, and average value at the top of bed (kg/kg of sand)
y = mass fraction of gas (kg/kg)
z = vertical coordinate (m)

Greek letters

β = fluid-particle interaction coefficient
ε = void fraction of bed (-)
ε_0 = initial void fraction of bed (-)
ε_{mf} = void fraction of bed at minimum fluidization condition (-)
γ = cone angle (°)
Λ = conductive heat transfer coefficient between adjacent streamlines (W/m.K)
λ_p = solid bulk viscosity (Pa.s)
μ_q = bulk viscosity of phase q (Pa.s)
$\tau_{q,z}$, $\tau_{q,r}$ = normal stress and shear stress of phase q (N/m^2)
ΔH_r = heat of pyrolysis reaction (J/kg)

Subscripts

a = annulus
f = fountain core
mf = minimum fluidization conditions
p = particles
s = spout
sand = sand particles
t = PET materials

Literature Cited

1. Erkiaga A, Lopez G, Amutio M, Bilbao J, Olazar M. Influence of operating conditions on the steam gasification of biomass in a conical spouted bed reactor. *Chem Eng J*. 2014;237:259–267.
2. Olazar M, Aguado R, Velez D, Arabiourrutia M, Bilbao J. Kinetics of scrap tire pyrolysis in a conical spouted bed reactor. *Ind Eng Chem Res*. 2005;44:3918–3924.
3. Epstein N, Grace JR. *Spouted and Spout-Fluid Beds-Fundamentals and Applications*. UK: Cambridge University Press, 2011.
4. Aguado R, Olazar M, Gaisán B, Prieto R, Bilbao J. Kinetic study of polyolefin pyrolysis in a conical spouted bed reactor. *Ind Eng Chem Res*. 2002;41:4559–4566.
5. Olazar M, Lopez G, Arabiourrutia M, Elordi G, Aguado R, Bilbao J. Kinetic modelling of tyre pyrolysis in a conical spouted bed reactor. *J Anal Appl Pyrolysis*. 2008;81:127–132.
6. Aguado R, Olazar M, Gaisán B, Prieto R, Bilbao J. Kinetics of polystyrene pyrolysis in a conical spouted bed reactor. *Chem Eng J*. 2003;92:91–99.
7. Elordi G, Lopez G, Olazar M, Aguado R, Bilbao J. Product distribution modelling in the thermal pyrolysis of high density polyethylene. *J Hazard Mater*. 2007;144(3):708–714.
8. Aguado R, Olazar M, San Jose MJ, Gaisán B, Bilbao J. Wax formation in the pyrolysis of polyolefins in a conical spouted bed reactor. *Energy Fuels*. 2002;16:1429–1437.
9. Arabiourrutia M, Lopez G, Elordi G, Olazar M, Aguado R, Bilbao J. Characterization of the liquid obtained in tyre pyrolysis in a conical spouted bed reactor. *Int J Chem Reactor Eng*. 2007;5:12–25.
10. Arabiourrutia M, Lopez G, Elordi G, Olazar M, Aguado R, Bilbao J. Product distribution obtained in the pyrolysis of tyres in a conical spouted bed reactor. *Chem Eng Sci*. 2007;62:5271–5275.
11. Artetxe M, Lopez G, Amutio M, Elordi G, Olazar M, Bilbao J. Operating conditions for the pyrolysis of Poly-(ethylene

terephthalate) in a conical spouted-bed reactor. *Ind Eng Chem Res*. 2010;49:2064–2069.
12. Elordi G, Olazar M, Lopez G, Amutio M, Artetxe M, Aguado R, Bilbao J. Catalytic pyrolysis of HDPE in continuous mode over zeolite catalysts in a conical spouted bed reactor. *J Anal Appl Pyrolysis*. 2009;85:345–351.
13. López G, Olazar M, Aguado R, Bilbao J. Continuous pyrolysis of waste tyres in a conical spouted bed reactor. *Fuel*. 2010;89:1946–1952.
14. Lopez G, Olazar M, Aguado R, Elordi G, Amutio M, Artetxe M, Bilbao J. Vacuum pyrolysis of waste tires by continuously feeding into a conical spouted bed reactor. *Ind Eng Chem Res*. 2010;49:8990–8997.
15. Hosseini SH, Ahmadi G, Olazar M. CFD simulation of cylindrical spouted beds by the kinetic theory of granular flow. *Powder Technol*. 2013;246:303–316.
16. Bao X, Du W, Xu J. An overview on the recent advances in computational fluid dynamics simulation of spouted beds. *Can J Chem Eng*. 2013;91(11):1822–1836.
17. Madhiyanon T, Soponronnarit S, Tia W. A mathematical model for continuous drying of grains in a spouted bed dryer. *Drying Technol: Int J*. 2002;20(3):587–614.
18. Niksiar A, Sohrabi M, Rahimi A. A model for the dynamics of spouted bed dryers. *Drying Technol: Int J*. 2013;31(3):295–307.
19. Olazar M, Lopez G, Altzibar H, Bilbao J. Modelling batch drying of sand in a draft-tube conical spouted bed. *Chem Eng Res Design*. 2011;89(10):2054–2062.
20. Ghalavand Y, Rahimi A, Hatamipour MS. Experimental study and mathematical modeling of green pea drying in a spouted bed. *Drying Technol: Int J*. 2012;30(2):128–137.
21. Lim CJ, Lucas JP, Haji-Sulaiman M, Watkinson AP. A mathematical model of a spouted bed gasifier. *Can J Chem Eng* 1991;69(2):596–606.
22. Lucas JP, Lim CJ, Watkinson AP. A nonisothermal model of a spouted bed gasifier. *Fuel*. 1998;77(7):683–694.
23. Mendes A, Dollet A, Ablitzer C, Perrais C, Flamant G. Numerical simulation of reactive transfers in spouted beds at high temperature: Application to coal gasification. *J Anal Appl Pyrolysis*. 2008;82(1):117–128.
24. Sanchez I, Mazza G, Flamant G, Gauthier D. A streamtube nonisothermal spouted-bed reactor mathematical model. *Chem Eng Sci*. 2000;55(1):193–202.
25. Rahimi A, Hatamipour MS, Gholami M, Haghnegahdar MR. Nonisothermal modeling of the flue gas desulphurization process using a semi-dry spouted bed reactor. *Chem Eng Res Design*. 2011;89(6):777–784.
26. Moeini M, Hatamipour MS. Flue gas desulfurization by a powder-particle spouted bed. *Chem Eng Technol*. 2008;31(1):71–82.
27. Tao M, Jin B, Zhong W, Yang Y, Xiao R. Modeling and experimental study on multi-level humidifying of the underfeed circulating spouted bed for flue gas desulfurization. *Powder Technol*. 2010;198(1):93–100.
28. Niksiar A, Sohrabi M. Mathematical modeling of waste plastic pyrolysis in conical spouted beds: Heat, mass and momentum transport. *J Anal Appl Pyrolysis*. 2014;110:66–78.
29. Niksiar A, Sohrabi M, Rahimi A. Comparative evaluation of existing correlations to predict spouted bed hydrodynamics. *Drying Technol*. 2013;31(9):975–989.
30. Yoshioka T, Grause G, Eger C, Kaminsky W, Okuwaki A. Pyrolysis of poly(ethylene terephthalate) in a fluidised bed plant. *Polymer Degrad Stab*. 2004;86(3):499–504.
31. Lim CJ, Mathur KB. A flow model for gas movement in spouted beds. *AIChE J*. 1976;22(4):674–680.
32. Niksiar A, Sohrabi M, Rahimi A. A correction on a one-dimensional model for conical spouted beds published in chemical engineering and processing, 48 (2009) 1264–1269. *Chem Eng Process: Process Intensification*. 2013;70:289–291.
33. Gidaspow D. *Multiphase Flow and Fluidization*. San Diego: Academic Press, 1994.
34. Wen CY, Yu YH. Mechanics of fluidization. *Chem Eng Prog Symp Series*. 1966;62(2):100–111.
35. Ergun S. Fluid flow through packed columns. *Chem Eng Prog*. 1952;48:89–94.
36. Schiller L, Naumann Z. A drag coefficient correlation. *Verein Deutscher Ingenieure*. 1935;77:318.
37. Brems A, Baeyens J, Vandecasteele C, Dewil R. Polymeric cracking of waste polyethylene terephthalate to chemicals and energy. *J Air Waste Manag Assoc*. 2011;61(7):721–731.
38. Rowe PN, Claxton KT. Heat and mass transfer from a single sphere to flowing through an array. *Trans Inst Chem Eng*. 1965;43:T321.
39. Handley D, Heggs PJ. Momentum and heat transfer mechanisms in regularly shaped packings. *Trans Inst Chem Eng*. 1968;46:T251–T264.
40. Mazza GD, Barreto GF. Analysis of models for heat transfer between gas-fluidized beds and immersed surfaces at high temperatures. *Powder Technol*. 1993;75(2):173–179.
41. Kunii D, Smith JM. Heat transfer characteristics of porous rocks. *AIChE J*. 1960;6(1):71–78.
42. Makibar J, Fernandez-Akarregi AR, Diaz L, Lopez G, Olazar M. Pilot scale conical spouted bed pyrolysis reactor: Draft tube selection and hydrodynamic performance. *Powder Technol*. 2012;219:49–58.

Manuscript received Oct. 12, 2014, and revision received Feb. 11, 2015.